Self-centering and damping capabilities of a tension-compression device equipped with superelastic NiTi wires

2015 Smart Mater. Struct. 24 075005

(http://iopscience.iop.org/0964-1726/24/7/075005)

Smart Mater. Struct. **24** (2015) 075005 (13pp)

doi:10.1088/0964-1726/24/7/075005

Self-centering and damping capabilities of a tension-compression device equipped with superelastic NiTi wires

H Soul[1] and A Yawny[1,2]

[1] CONICET, Division Metales, Centro Atómico Bariloche (CNEA), Instituto Balseiro (UNCuyo), Bustillo 9500, (8400) San Carlos de Bariloche, Argentina
[2] CNEA, División Metales, Centro Atómico Bariloche (CNEA), Instituto Balseiro (UNCuyo) Bustillo 9500, (8400) San Carlos de Bariloche, Argentina

E-mail: hugo.soul@gmail.com

Received 14 January 2015, revised 26 March 2015
Accepted for publication 14 April 2015
Published 3 June 2015

Abstract

The hysteretic damping capacity and high recoverable strains characterizing the superelastic response of shape memory alloys (SMA) make these materials attractive for protection systems of structures subjected to dynamic loads. A successful implementation however is conditioned by functional fatigue exhibited by the SMA when subjected to cyclic loading. The residual deformation upon cycling and the efficiency in material usage are the two most restrictive issues in this sense. In this paper, a device equipped with superelastic NiTi SMA wires and capable of supporting external tension compression loads with optimized properties is presented. It is shown how the introduction of the wires' pre-straining allows for the absorption of deleterious residual deformation without affecting the self-centering capabilities upon unloading, in contrast with what occurs for pre-strained tendons. These features were experimentally verified in an in-scale prototype composed of two 1.2 mm diameter superelastic NiTi SMA wires. In order to numerically assess the dynamic response of a simple structure subjected to seismic excitations, a multilinear superelasticity model for the NiTi wires was developed.

S Online supplementary data available from stacks.iop.org/SMS/24/075005/mmedia

Keywords: self-centering, damping, device characterization, seismic isolation

(Some figures may appear in colour only in the online journal)

1. Introduction

The superelastic effect is a particular behavior exhibited by shape memory alloys (SMAs) subjected to mechanical loading by which a martensitic transformation is induced once stress reaches a critical value and reversed when the load is relaxed [1]. A superelastic cycle presents several features which make SMAs attractive for use as kernel elements in protection systems for structures subjected to dynamical loads [2]. The associated stress-strain hysteresis provides energy dissipation. The effective stiffness drop associated with the forward transformation plateau limits the load transfer from the floor to the protected structure. Additionally, the force exerted during reverse transformation provides an important restoring effect and reversible strains of 8–10% can be reached [3]. This characteristic provides self-centering capabilities to the protected structures which is an important factor for preventing excessive deformation and cumulative damage, for example, after an earthquake. This is remarked on in modern building codes [4, 5]. Self-centering capacity represents an important advantage of SMAs with respect to alternative hysteresis-based damping alternatives (e.g. controlled yielding members, friction braces, etc) [6].

The present work refers to the development of a device with superelastic NiTi SMA wires acting as kernel elements in passive protection systems exploiting both damping and self-centering capabilities. Among SMAs, commercial NiTi-based alloys exhibit one of the highest shape memory and superelastic strain recoveries and also acceptable fatigue, corrosion resistance and biocompatibility. Regarding the material geometry, as is pointed out in several research works [7–9], SMAs in wire or bar form are usually adopted for this kind of application. The main reasons are the efficient use of the material loading capacity associated with the uniform stress state upon uniaxial loading and the optimized manufacturing process, including continuous forming and thermal treatment operations which made possible the increasing of production rates with appreciably lowering costs [10]. As occurs with almost every practical implementation of a technological concept, problems associated with the concrete use of materials arise, creating the need for further research. SMAs in general, but NiTi alloys in particular, exhibit functional fatigue which results in a decrease of hysteresis and the accumulation of residual strains upon superelastic cycling [11–13]. A difficulty concerning the use of wires or bars under uniaxial loadings is the large lengths required for guarantying an acceptable displacement capacity (device stroke). Another drawback affecting slender elements like wires is that they can be loaded only under tension and are unstable under compression loadings (buckling). Therefore, pairs of wires have to be frequently disposed of as tendons in symmetrical configurations [14, 15] with them being loaded alternatively in each hemicycle with the consequent negative impact in material usage efficiency.

Research efforts in the materials science field include either the development of novel SMA systems [16, 17] or the microstructural optimization of already existing materials [18, 19], seeking a more stable superelastic behavior, improved dissipative and strain recovery capabilities or lower costs. From the civil or mechanical engineering perspectives, technical solutions are proposed to achieve an efficient use of the available alloys in different scenarios. Dolce *et al* [20, 21] presented two different designs of devices capable of supporting external tension–compression loading by using NiTi wires under a special arrangement which favors either the dissipative or the self-centering properties of superelasticity. Several dynamical response experiments were carried out to demonstrate their beneficial effect in restrainer's applications for isolated structures [20] and in braces in framed in-scale building structures [21]. A similar design was proposed by Parulekar *et al* [22] who compared the performances with devices working on the principle of plastic yielding. Han *et al* [23] developed and tested a device equipped with NiTi wires which is capable of supporting tension, compression and torsion loadings. Attanasi *et al* [9] numerically characterized the performance of a multidirectional device composed of eight NiTi springs, demonstrating the possibilities of such particular geometrical arrangement. Speicher *et al* [24] designed a damper based on a NiTi Belleville washer pile-up. These last two works are examples of alternatives to the uniaxial type of simple loading commented on so far.

The device presented in the present work is of self-centering type and is inspired by the proposal of Dolce *et al* [20] that was introduced in the previous paragraph. One of the goals of the device proposed here is the improvement in material usage efficiency. This is possible due to a special design which results in the wires always acting under a tensile load, independent of whether the device external forces were tensile or compressive. By adding pre-straining capability, it is possible to improve the device performance by keeping the wires tightened during operation without compromising the restorative force exerted upon unloading. After a description of the device and its working principle, it is demonstrated how by pre-straining the NiTi wires above a certain level, the residual deformation associated with functional fatigue can be compensated for, thus avoiding their loosening during operation. The results of an experimental characterization performed with an in-scale prototype are then presented. Characterization included tests under cycling conditions for frequencies ranging from 0.001 to 5 Hz and amplitudes from 1 to 5 mm. The results were interpreted in terms of the coupling between thermal effects and the mechanical response [25–27]. Finally, a multilinear superelasticity model is developed and used to numerically study the mitigating effects on the dynamical response of a simple structure subjected to seismic excitation.

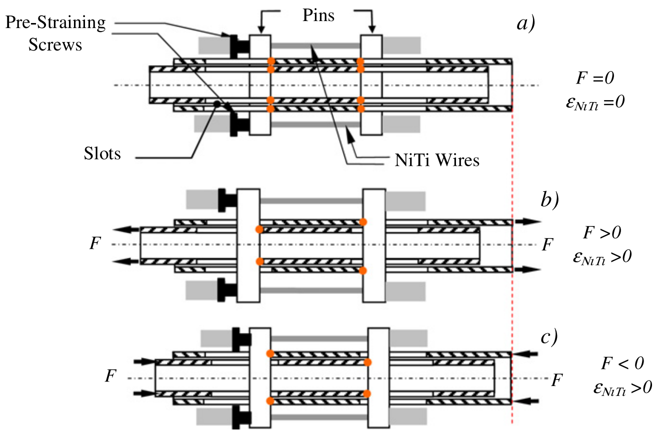

Figure 1. Schematic explanation of the device working principle (external tube position fixed, indicated by the vertical red dashed line at the right of the figure). (a) Initial condition upon mounting, no net external load; each pin is in contact simultaneously with both tubes. Relative displacement of the tubes moves the pins which in turn produces the straining of the NiTi wires. The wires are subjected to tension whenever the external force is positive (b) or negative (c), respectively.

2. Device functioning description

The functioning principle of the proposed device is explained with the aid of the schematic drawing presented in figure 1. The device is composed of two coaxial steel tubes, one sliding inside the other. The tubes are transversally crossed by two pins through longitudinal machined slots. Two superelastic NiTi wires are extended between the pins, one at each side of the tubes. Figure 1(a) illustrates the initial condition where the device is free of external loads. Dots are included in the drawings in figures 1(a)–(c) to denote the contact points between the pins' and the slots' ends along a complete working cycle. In figure 1(a), eight contact positions are

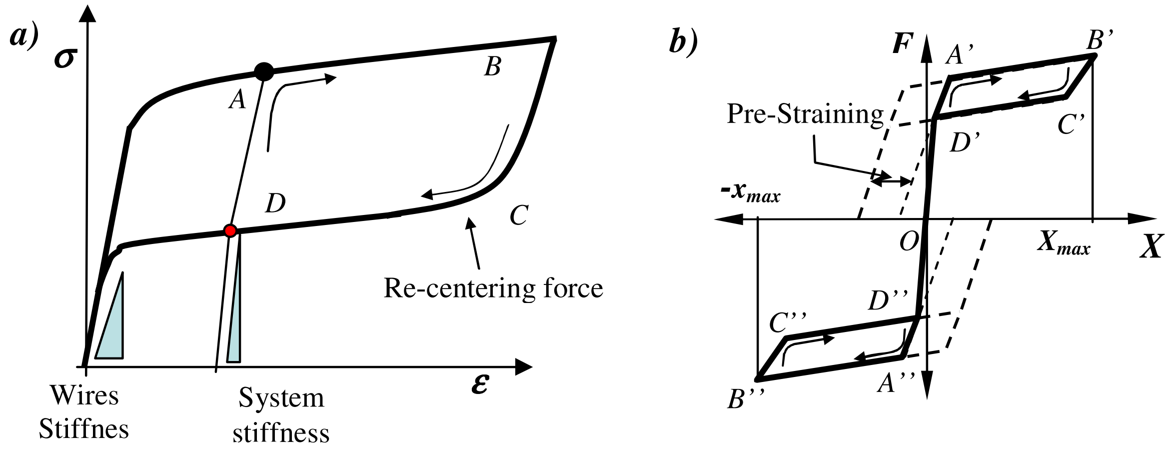

Figure 2. Pre-straining effect. (a) Wire pre-strained to point *A* will describe path *ABCD* while the initial portion of the cycle acts as a strain reservoir to compensate for posterior permanent strains. (b) The device performs a complete cycle described by the 'double flag' path *A′B′C′D′A′OA″B″C″D″* in the *F*–*X* diagram. Note that one tension–compression cycle of the device involves two cycles of the wire.

indicated. For the sake of a clear interpretation of displacements and force sense, the position of the external tube, indicated by the red dashed line, is kept fixed in figures 1(a)–(c). Upon application of an external tensile force, relative displacement of the tubes will occur as shown in figure 1(b). The four contact points indicated for this situation transmit the load to the pins resulting in the NiTi wires being stretched. The mechanism is constructed in such a way that whatever the sense of the relative tube displacement, the wires are always subjected to positive strains. This is depicted in figure 1(c) where the external force is now reversed. Each time the device position passes through the neutral position, referred to as the inversion point in the text and represented by the condition illustrated in figure 1(a), there is a change in the tube that pushes each pin. This can be appreciated by the change in the contact points acting in each case. In that way, for one cycle of the external force, the NiTi wires perform two complete superelastic cycles. Therefore, the force vs displacement (*F*–*X*) response of the whole device will describe a 'double flag' type of behavior [5, 20, 21] that will be better understood when describing figure 2.

By means of the pre-straining screws shown in figure 1(a) it is possible to apply a certain initial strain level to the wires during mounting. The effect on the device response is illustrated in figure 2. Assuming that both wires are pre-strained up to a strain level corresponding to point *A* in figure 2(a), *a posterior* complete symmetric oscillation of the device with an amplitude x_{max} will result in each wire following twice the partial superelastic trajectory *ABCD* depicted in figure 2(a). Thus, in the text a distinction will be made between wire cycles and device cycles. The corresponding force vs displacement *F*–*X* response of the whole device will follow the path denoted by *OA′B′C′D′OA″B″C″D″O* indicated in figure 2(b).

As the elastic slope around the inversion point is only determined by the pins and pin leans stiffness, the device would exhibit a high stiffness around this point. Due to that, it will provide a high restoring force close to the near zero position which results in a structure with self-centering capability. Moreover, it is expected that permanent strains that could have been accumulated upon cycling (typically reaching 2% [25, 28]) can be compensated for by providing suitable levels of pre-straining.

It is worth remarking here that a different effect will be observed in the case where the NiTi SMA wires were inserted in a structure as symmetrical tendons [14, 15], in the typical way illustrated in figure 3. In this case, pre-straining would result in an improvement of the hysteresis area and consequently on the dissipative capacity but to the severe detriment of the self-centering force, which would nearly vanish.

Based on conceptual considerations explained above, an in-scale prototype was manufactured and the results of its basic experimental characterization are provided in the following section.

3. Prototype and experimental characterization

A prototype device equipped with two NiTi wires was constructed and tested. Ni-rich (50.8 at.% Ni) 1.2 mm diameter superelastic NiTi wires in straight annealed condition were provided by Memory Metalle GmbH (now Memry GmbH). The austenite finish temperature A_f was −10 K with the wire exhibiting superelastic behavior at room temperature. Detailed information about transformation temperatures is provided elsewhere [11]. The prototype was designed for a nominal wire member length $L = 80$ mm, it being possible to compensate for small initial length differences with the pre-straining screws. The analysis of performance was carried out assuming the device will operate under standard ambient temperature. The characterization testing was performed at room temperature (22 °C) using a servo hydraulic testing machine MTS 810 with 100 kN maximum load capacity. Figure 4(a) illustrates the designed prototype with the different components while figure 4(b) shows the device set in the testing machine.

The experimental characterization program started by performing two cycling sequences aimed to demonstrate the

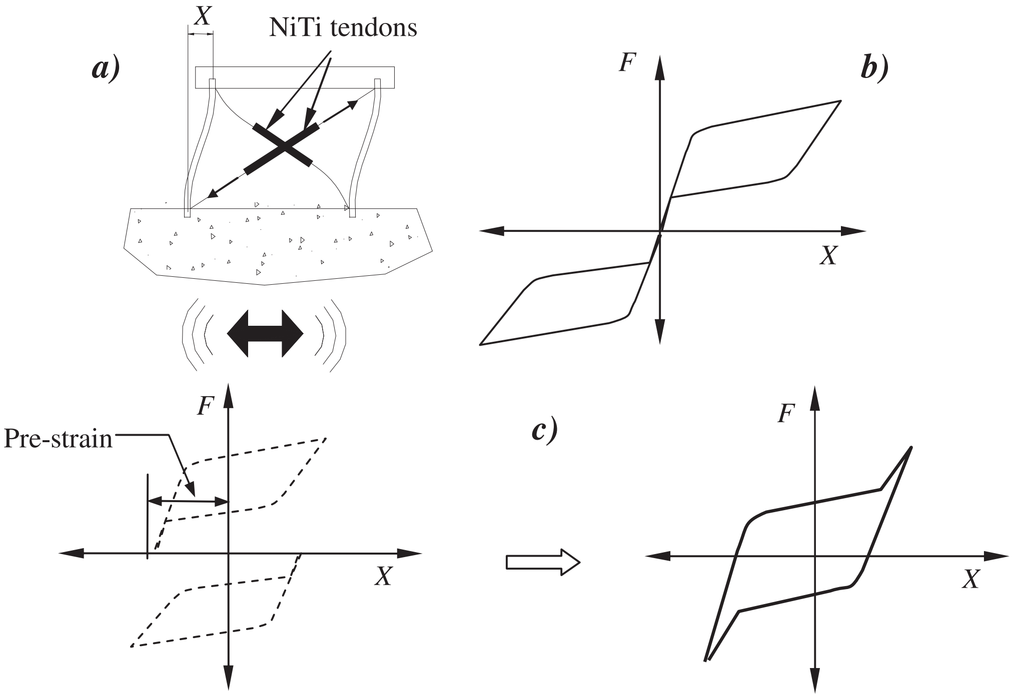

Figure 3. (a) Typical symmetric configuration of NiTi wires as metallic tendons in a flexible structure. (b) Double flag *F–X* response associated with the superelastic wires. (c) Schematic description of the pre-straining effect on this kind of structure showing how hysteresis is improved but to the detriment of the self-centering capability.

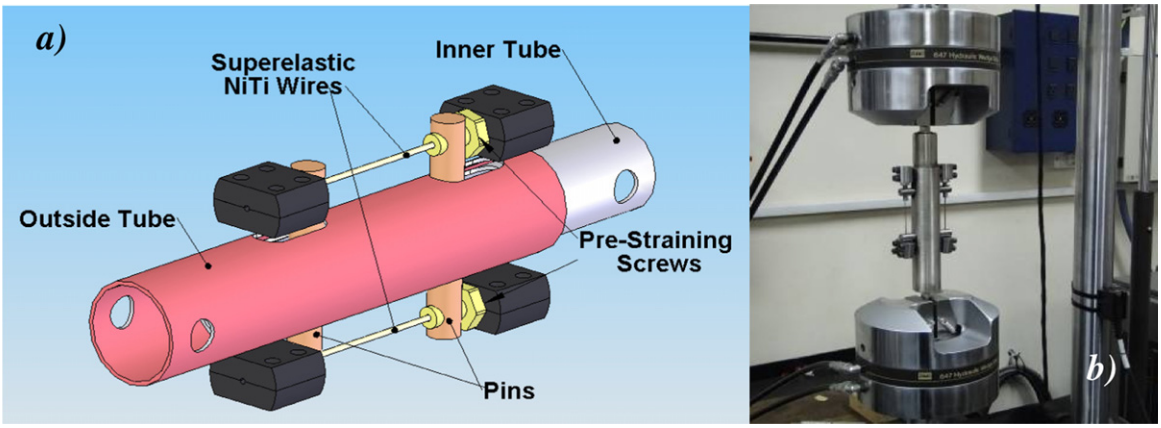

Figure 4. Designed prototype. (a) 3D schematic representation with the main components highlighted. (b) Prototype mounted on the testing machine.

effect of pre-straining on the device performance. In the first, the wire were just slightly tightened by the pre-straining screws while in the second, 2% pre-strain was applied. In both cases, a fresh pair of wire pieces was used. The device was subjected to a number of 50 fully reversed ramp cycles at a displacement rate of 1 mm min^{-1}. It is worth pointing out here that, due to the working principle involved, the NiTi wires actually perform 100 tensile cycles. Figures 5(a) and (b) show cycles 1 in red and cycle 50 in blue for both sequences (intermediate cycles are denoted in gray). The imposed maximum displacement amplitudes were defined such that full transformation of the NiTi wires was obtained. This can be appreciated by the small load increase observed at the end of the plateaus in both figures. Maximum displacements were thus set in 6.75 mm and 5 mm for the pre-strain free and the 2% pre-strained conditions, respectively.

The evolutions of the superelastic response observed in figure 5 are in line with previous studies on the effects of functional fatigue effects of similar superelastic NiTi wires [11, 12], i.e. a decrease of plateau stress levels, more marked for the upper plateau, and a tendency to a more stable behavior after 100 wire cycles are observed. The uneven drop in plateau stress levels results in turn in a decrease in the dissipated energy as shown in figure 6(a) where data corresponding to the two sequences shown in figure 5 are represented. Firstly, it is noted that the sequence without pre-strain exhibits a sort of noisy behavior with damping capacity values oscillating in a certain band after performing just a

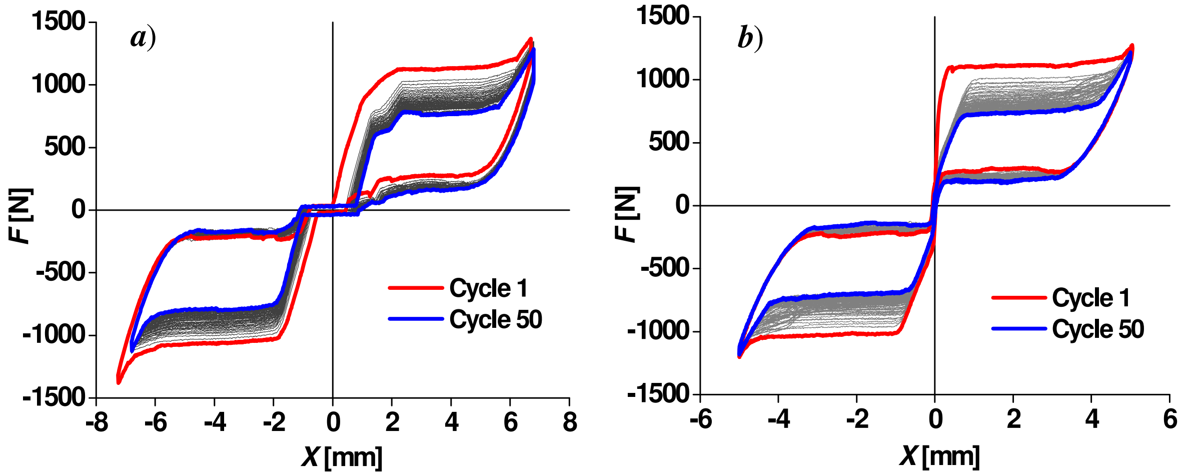

Figure 5. Evolution of the prototype response upon 50 constant displacement amplitude cycles (100 wire cycles). (a) Pre-strain free condition. (b) Wires with 2% pre-strain. Displacement rate was 1 mm min^{-1} in both cases.

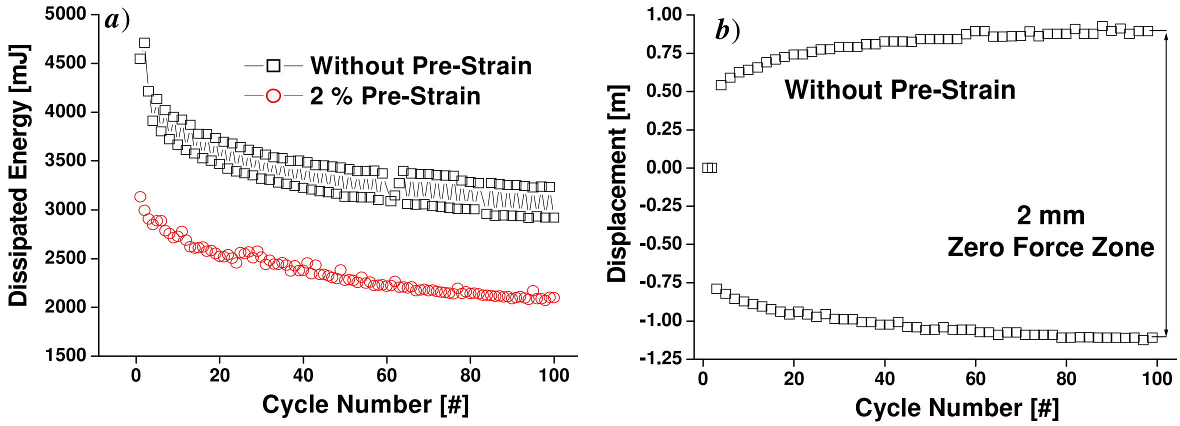

Figure 6. (a) Evolution of the dissipated energy per wire cycle during the first 100 wire cycles (50 device cycles). (b) Displacement limits associated with the development of a zero force zone for the pre-strain free case.

couple of cycles. This effect is a result of the accumulation of residual deformation upon cycling resulting in a gradually developing zero-force zone around the inversion point. A consequence of this is that wires become loosened and pins detach from their leans, favoring their crossing and uneven straining.

The evolution of the displacement limits denoting the extension of the zero-force zone is illustrated in figure 6(b) where it can be seen that a 2 mm width zero-force zone develops around the inversion point after 100 wire cycles. The width of the dead zone can be considered a good indicator of the degree of pre-straining that has to be applied to avoid wire loosening with further cycling. In fact, this was the case for the cycling sequence corresponding to wires with a pre-strain of 2% included in figure 6(a) where the appearance of a zero force zone was now completely avoided. The absolute value of dissipated energy is lower in the case of the pre-strain free situation due to the reduced wire active length available. Both sequences exhibit however the same decreasing evolution upon cycling.

As can be noted from the previous figures, the first 100 cycles result in the wires exhibiting more stable behavior. This is usually referred as 'stabilization training' and represents an alternative procedure for reducing the development of a zero force zone, at the expense of greater complexity and cost.

The experimental program continued with the characterization of the frequency response. After the training stage described in the previous paragraph, the performance of the prototype was tested for 12 frequencies in the range of 0.001 to 5 Hz using displacement amplitudes of 1, 2, 3, 4 and 5 mm. This totalizes a number of 60 tests for each of the considered conditions, i.e. without and with pre-strain. Results are reported here only for the prototype with the pre-strained condition because no relevant differences were found between them. Representative results are shown in figure 7 where for the sake of clarity only curves corresponding to the first cycle for each of the considered amplitudes have been included in the plots.

As can be observed from the figure, there exists a strong dependence of the shape of the cycles on the frequency. This can be quantitatively described by characterization parameters like the energy dissipated in a whole cycle of the device

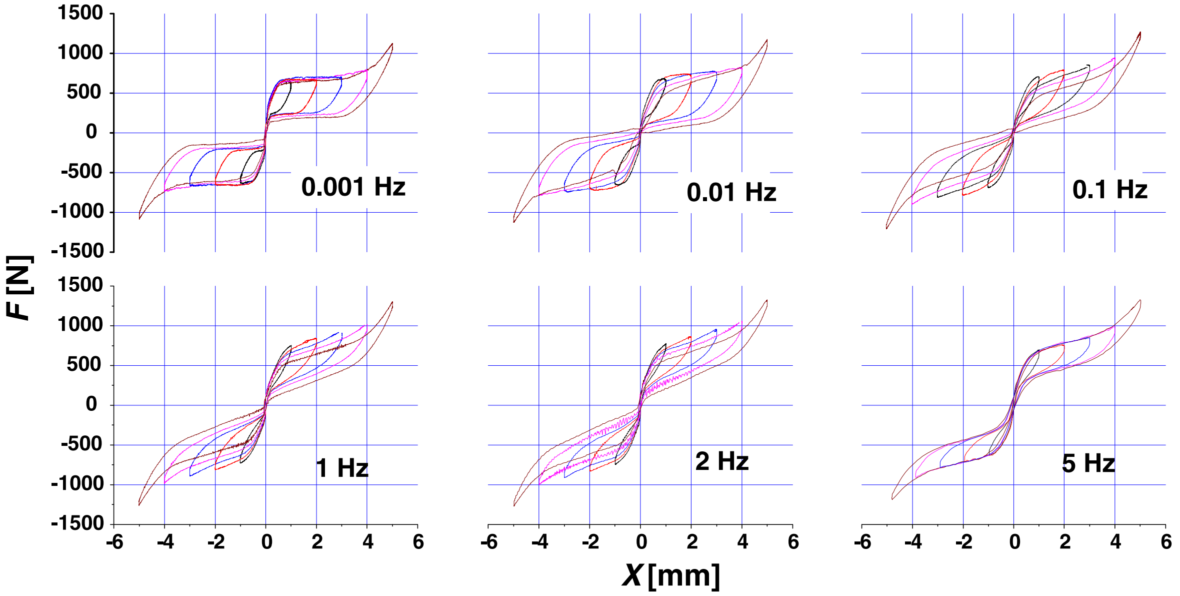

Figure 7. Summary of the results for 6 of the 12 tested frequencies. The individual curves represent the device response corresponding to the first cycle for each combination of frequency and displacement amplitude considered. The different colored curves correspond to the different amplitudes of 1, 2, 3, 4 and 5 mm imposed on the tests.

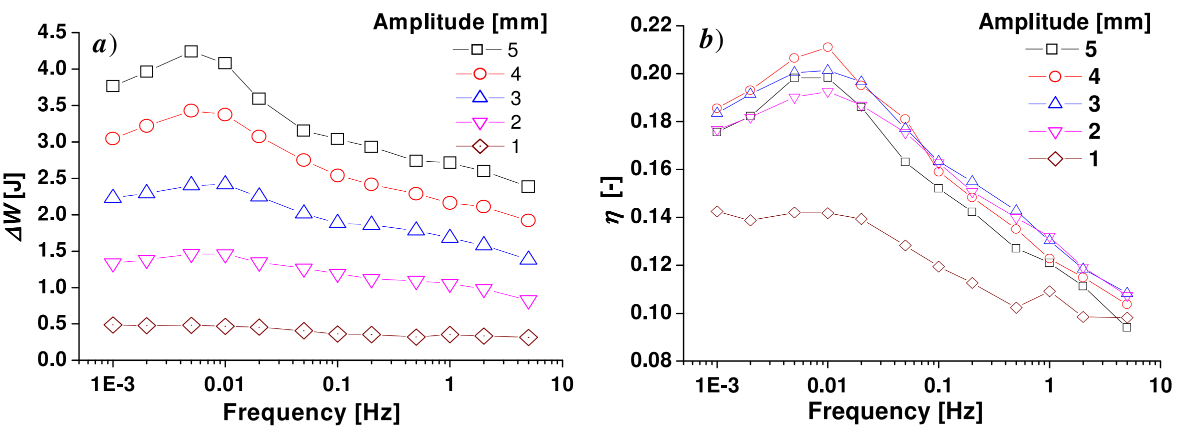

Figure 8. Representation of the test results as a function of the cycling frequency. (a) Energy dissipated ΔW and (b) loss factor η.

(hereafter ΔW), and the loss factor η defined as:

$$\eta = \frac{\Delta W}{2\pi W}, \tag{1}$$

where W is the strain work measured at the maximum displacement amplitude of the cycle. This last definition result is somewhat arbitrary, and alternative definitions can be found in the literature, based upon the maximum stored energy or a quasi-elastic work calculated using a secant modulus [29]. However, the definition of the η factor adopted here allows for an easier comparison with the same factor defined for other materials or damping mechanisms [30]. In figures 8(a) and (b), the frequency dependence of ΔW and η corresponding to the different amplitudes are presented. A non-monotonic trend is obtained for both parameters, with a maximum developed around 0.01 Hz. This behavior is related to the coupling between the mechanical response and the thermal effects arising from the transformation enthalpy associated with the first order martensitic phase transformation involved and also with the temperature dependence of the critical stress for transformation (Clausius–Clapeyron relationship), as has been explained elsewhere [25, 26]. The alternative representation given in figure 9 might be also illustrative. It can be seen that the amplitude dependency is approximately linear for ΔW and somewhat weaker for η. Therefore, for amplitudes above 1 mm (equivalent to 1.25% strain) it is possible to associate each tested frequency with a unique value of the loss factor η.

In figure 10, the frequency dependence of two additional parameters was evaluated: the stiffness associated with the forward transformation and the value of the force at the end of the reverse transformation. The forward transformation stiffness can be conceived as the post-yielding stiffness of isolator devices [4]. This post-yielding stiffness, associated with a structural mass M defines a post-yielding period $T_P = 2\pi \cdot (M/E_{Tr})^{1/2}$ which is utilized in several building codes (e.g. AASHTO [31]) to characterize the capacity of isolators in limiting load transfer to a structure. In this case, the stiffness

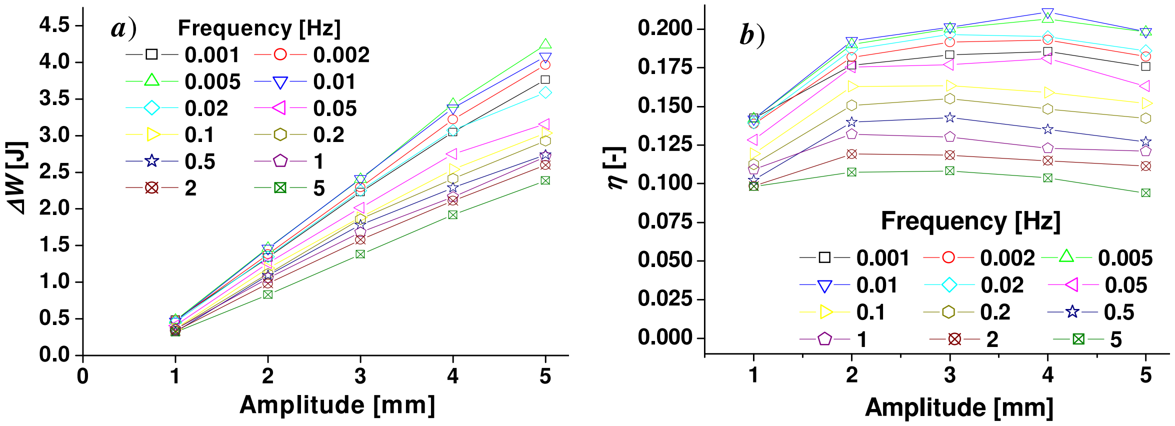

Figure 9. Representation of the test results as a function of the cycling amplitude. (a) Energy dissipated ΔW and (b) loss factor η.

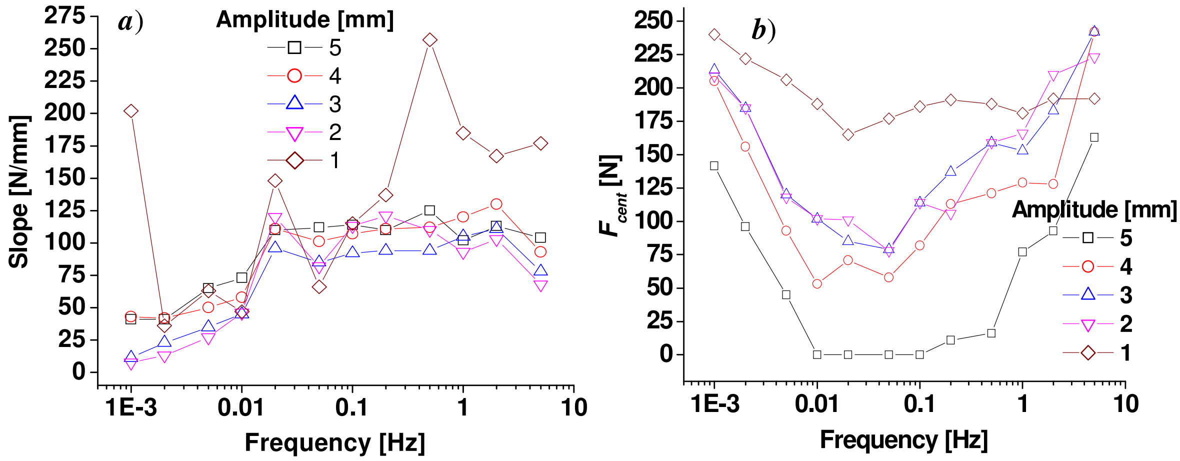

Figure 10. Characterization test results represented as a function of the cycling frequency. (a) Stiffness along the forward transformation. (b) Restoring force at the end of the reverse transformation F_{cent}.

was determined by a linear fitting of F–X curve along the forward transformation plateau between 0.75 mm and the maximum displacement limit, excepting for the 5 mm amplitude cycles for which the range 0.75–4 mm was considered for the fitting. The evaluation of the force upon reverse transformation was included in order to characterize the feasible maximum restoring values that could be reached under different tested cycling conditions. This capacity, together with the re-stiffening at the end of transformation, is unique for SMA superelastic materials and cannot be found in other materials exploited in anti-seismic protective systems.

Regarding the transformation stiffness (figure 10(a)), there is no clear trend followed by the points. Roughly, the stiffness increases up to 0.01 Hz and exhibits a tendency to saturation at values around 100 N mm^{-1}.

The restoring force F_{cent} (figure 10(b)) exhibits an inverted bell shape behavior, with a drop at intermediate frequencies, it being more pronounced the higher the amplitude is. This behavior can also be rationalized by considering the thermal effects mentioned before to rationalize the frequency dependence of ΔW and η.

The parameters evaluated up to this point describe superelastic behavior for the first cycle of each experiment. In contrast, the final step of the experimental program addressed the evolution of the superelastic behavior upon sustained cycling for fixed frequency and amplitude. As was the case in the previous characterization stage, here the experiments were performed on wires in the stabilized condition. The evolutions studied in this step are reversible and are also related to the heat effects associated with the first order stress induced martensitic phase transformation, responsible for the particular behavior of SMAs. Superelastic cycling at constant frequency and amplitude will result in a transient during which the maximum and minimum forces vary as a consequence of the NiTi wire temperature change determined by the balance between the irreversible cyclic work and the heat dissipated to the surroundings [32, 33]. The effect can be appreciated in figure 11 where the device force response vs time is presented for five different imposed displacement amplitudes and three frequencies. It can be seen that the transient effect is particularly detectable for the highest amplitudes and frequencies.

This transient stage is also responsible for the effect detected in figure 8(a) where it was observed that the higher the frequency and amplitude, the more noticeable the

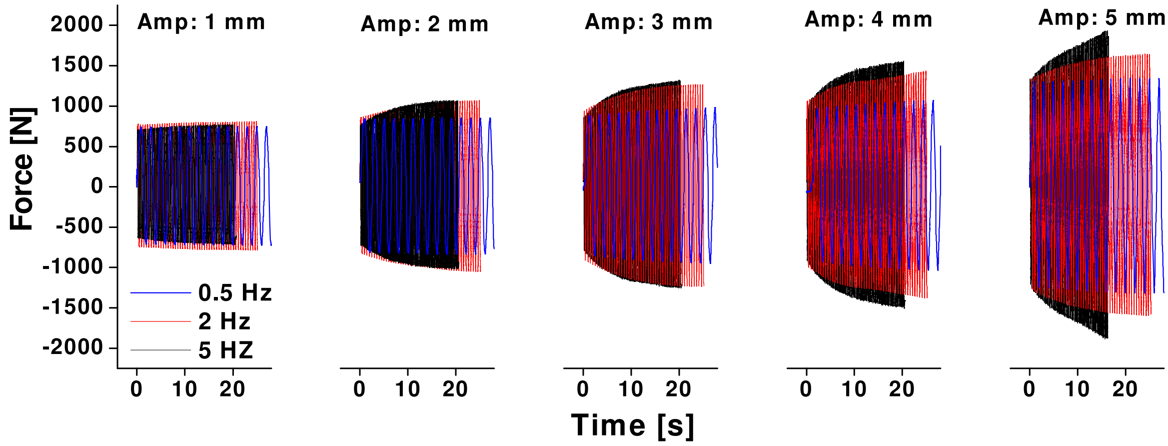

Figure 11. Evolution of the force with time associated with the transient effect for 0.5, 2 and 5 Hz.

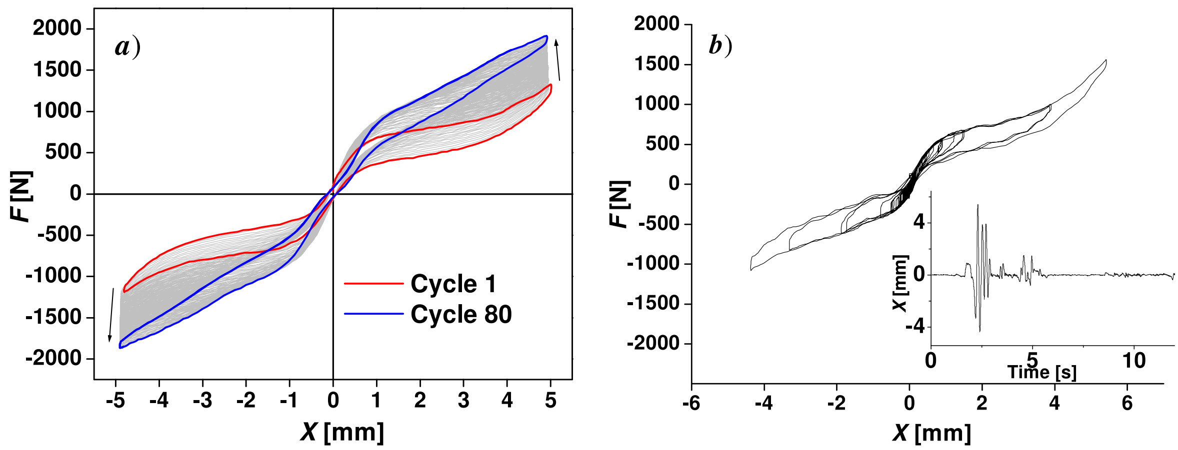

Figure 12. (a) Cycle evolution due the transient effect for the 5 Hz–5 mm amplitude test. (b) Superelastic cycles obtained for a displacement program corresponding to a typical seismic response.

difference between ΔW values corresponding to the first and last cycle of the sequence.

The changes occurring in the shape of the superelastic cycles corresponding to the experiments presented in figure 11 are illustrated in figure 12(a). Results of the test performed at 5 Hz with an amplitude of 5 mm were included. Both figures 11 and 12(a) reflect the magnitude of the changes associated with the transient effect. For applications requiring sustained high amplitude and frequency cycling, a more extensive characterization is necessary including not only frequency dependence but also environment heat transfer convective conditions (see Sun *et al*'s work [32] for NiTi thin wires).

The present work is focused on the responses of structures to seismic inputs, usually consisting in a reduced number of cycles whose amplitudes are rapidly reduced. Therefore, it would be interesting to have an indication of whether the just characterized thermal transients will have an influence in such a short term type of application. In figure 12(b), the response of the device to the displacement program indicated in the minor axis inset graphs is presented. This displacement program corresponds to the simulated response of a structure to the acceleration record of the N-S component of the 'El Centro' earthquake, 1942. As can be observed from the device response, no evident influence of transient effects could be detected. This result allows one to conclude that all the relevant information for the analysis of the seismic response of the device is basically contained in the first cycle. Based on that conclusion, the transient effect will be neglected in the superelastic behavior model introduced in the next section.

4. Performance analysis

Parameters such as the dissipated energy per cycle ΔW, the loss factor η and the restoring force F_{cent} describe quantitatively important aspects of the device performance. They may be used either for the comparison among devices based on different working principles or they can be introduced in linearized schemes to estimate device response to simple harmonic excitations. However, when more complex inputs like those associated with seismic ground motion are considered, a numerical approach arises as a more appropriate tool for the correct evaluation of the effect of the device on the structural response. In this section, a time history analysis

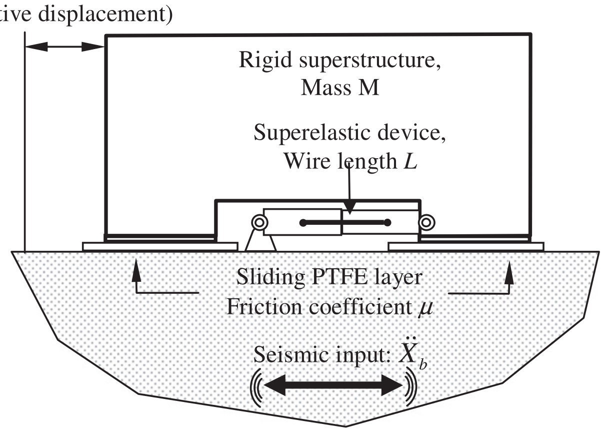

Figure 13. Schematic representation of the model one-degree-of-freedom structure considered for the numerical simulation.

is performed to numerically evaluate the dynamical response of a simple one-degree-of-freedom model structure subjected to a seismic type of excitation expressed in terms of the floor acceleration $\ddot{X}_b$.

The model structure considered consists of a monolithic mass M resting on a flat PTFE layer attached to the floor as is represented in figure 13. The arrangement can be viewed as an isolated structure for which relative displacements concentrates in the sliding surface between the mass and the PTFE layer where Coulomb type friction with a coefficient $\mu = 0.04$ is assumed [34]. In figure 14, the F–X between mass and PTFE layers plus the double-flag device action is represented. The analysis of friction forces should include the contribution of friction between the coaxial tubes. This force depends on manufacturing quality and mounting procedures while the friction originated in the PTFE layers is proportional to the mass M. Even though their different origins, in the schematic representation of figure 14 the tube-to-tube device friction was included as part of the total friction force acting on the system.

For the analysis of the dynamical response, the superelastic behavior of NiTi wires is introduced by using the multilinear model detailed in figure 15. Position and slope of the linear segments are adjusted with six parameters: elastic modulus of austenite E_A and martensite E_M, transformational modulus E_{Tr}, transformation strain ε_T, hysteresis stress width σ_{HYS} and upper plateau critical transformation stress σ_{CR}. Simulations were repeated for the two sets of parameters referred to as P1 and P2 and detailed in table 1. They have been selected by fitting experimental curves from the previous tests obtained at frequencies of 5 and 0.001 Hz (the two extremes of the tested frequency range), respectively. Since no thermal coupling effects are considered, this model is not able to reflect the superelastic behavior under testing conditions different from those under which the parameters were selected. Effects related to sustained cycling will also not be reproduced by this simple mechanical model. The adoption of such a simplified approach is justified by the particular characteristics of the problem studied here, i.e. few

Table 1. Model parameters.

	P1	P2
E_A (GPa)	30	50
E_M (GPa)	14.25	20
E_{Tr} (GPa)	3.8	1.17
σ_{CR} (MPa)	275	262
σ_{HYS} (MPa)	93	175
ε_T (-)	0.023	0.039

transformation cycles of diminishing amplitudes. Aside from the assessment of dynamical responses, the differences between results obtained with P1 or P2 can clarify the necessity of considering the frequency dependence of the superelastic behavior, which would require introducing more complex material models (e.g. thermomechanical models). In figures 16(a) and (b), the modeled cycles are superposed to the corresponding experimental ones. It can be seen that an adequate reproducibility has been obtained.

The response of the system is evaluated by stating the dynamical equilibrium of the NiTi wires and friction forces acting on the moving mass M:

$$F_{NiTi} + F_{fric} + M\ddot{X}_{abs} = 0, \tag{2}$$

where the total friction force F_{fric} is expressed as the sum of tube-to-tube device friction f and the corresponding to the sliding PTFE layers μM:

$$2A_{NiTi}\sigma_{NiTi}\,\mathrm{sgn}(X) + (\mu M + f)\,\mathrm{sgn}(\dot{X}) + M\ddot{X}_{Abs} = 0 \tag{3}$$

$$2A_{NiTi}\sigma_{NiTi}\,\mathrm{sgn}(X) + (\mu M + f)\,\mathrm{sgn}(\dot{X}) + M\ddot{X} = -M\ddot{X}_b \tag{4}$$

Here, X_{abs} corresponds to the mass coordinate measured from an inertial reference frame (i.e. $X_{abs} = X + X_b$). σ_{NiTi} and X_{NiTi} correspond to the uniaxial stress and transversal section of the wires respectively. For the simulations, the value of f was estimated in 30 N. Equation (4) is solved numerically following the Newmark method [35]. The kernel of the procedure is to calculate, given a displacement increment, the corresponding increment in σ_{NiTi}:

$$\Delta\sigma_{NiTi} = E_{NiTi}\Delta\varepsilon = \frac{E_{NiTi}}{L}\Delta X \cdot \mathrm{sgn}(X) \tag{5}$$

The effective modulus of NiTi wires E_{NiTi} depends on whether the wires are transforming or strained elastically. For the elastics case, E_{NiTi} is calculated assuming that the wires are composed of austenite and martensite portions serially connected. The martensite portion Z can be determined from the current σ, ε state:

$$Z = \frac{(\varepsilon - \sigma/E_A)}{\sigma/E_M + \varepsilon_t - \sigma/E_A}. \tag{6}$$

Then, a direct expression for E_{NiTi} results:

$$E_{NiTi} = \frac{E_A E_M}{E_A Z + E_M(1 - Z)}. \tag{7}$$

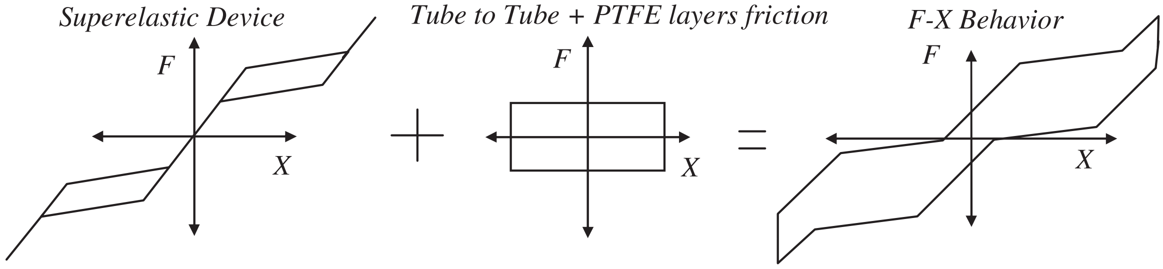

Figure 14. Schematic *F–X* behavior of the model structure obtained by superposition of the individual responses of the superelastic device and the friction contributions.

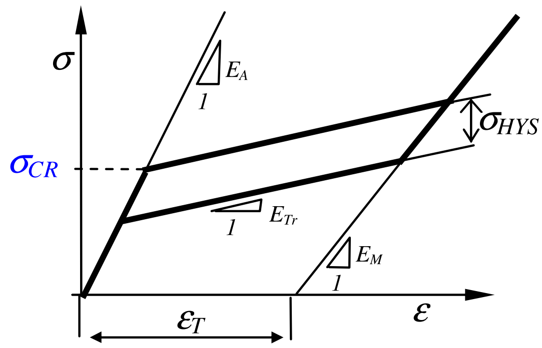

Figure 15. Multilinear model describing the superleastic effect of NiTi SMA.

Whenever the algorithm detects that E_{NiTi} will change in the current step, it is recalculated in order to find the exact instant (within a tolerance) of the transition point. In this way, it is possible to avoid the accumulation of numerical error in elastic-transformation transitions and in velocity sign changes.

For the seismic input, the accelerogram corresponding to the Northridge earthquake, 17 January 1994, recorded at the Jensen Filter Plant Station situated 12.97 km from the epicenter [36] was considered (figure 17(a)). A maximum peak ground acceleration of 9.98 m s^{-2} was detected. Assuming a mass M of 200 kg, the displacement followed by the bare model structure, i.e. without including the NiTi prototype, is shown in figure 17(b). A maximum displacement magnitude of 0.206 m can be observed. It is important to note also that after the Earthquake action, the mass resting position is 0.063 m which represents approximately 30% of the maximum registered displacement.

The response of the model structure is now calculated considering the introduction of the device equipped with NiTi wires of length $L = 2$ m. The obtained results are summarized in figure 18 where the relative mass displacements and the absolute accelerations for both sets of parameters P1 and P2 are represented. For comparison purposes, together with each calculated response (black line), the response of the structure obtained with a fully elastic device is included (blue line). The stiffness considered for the elastic device is equivalent to the initial stiffness of the superelastic device.

The relative displacements obtained for both the P1 and P2 sets of parameters are not reduced with respect to those obtained with fully elastic wires. However, the reducing effect is clear when comparing the resulting amplitudes with those obtained in the structure without the damping device (figure 17(b)). A very small residual displacement is obtained at the end of the ground excitation for both assumed superelastic behaviors. Focusing now in the absolute accelerations of the mass M, it can be seen that the superelastic device resulted in reducing peak ground acceleration from 10 m s^{-2} to 6 m s^{-2} for P1 and 4 m s^{-2} for P2, respectively. This reduction effect is higher in comparison with accelerations

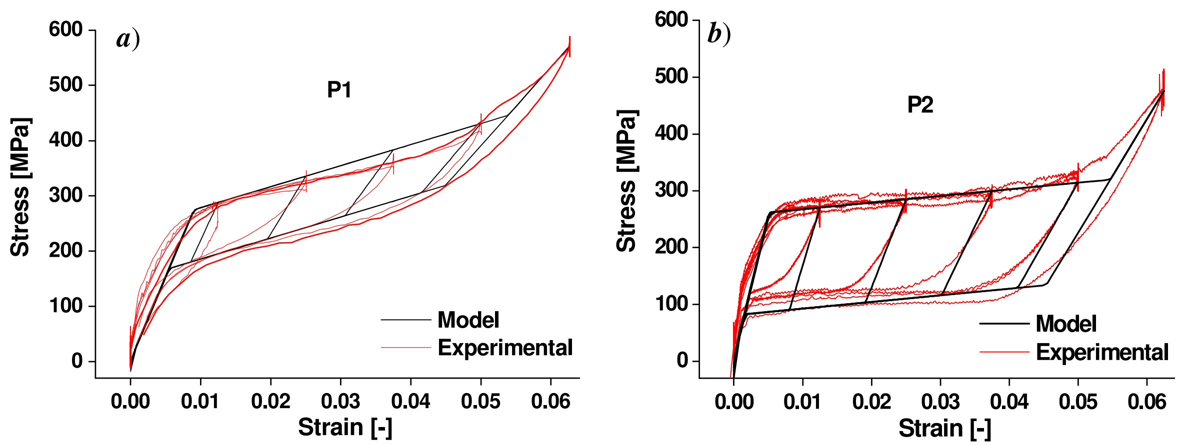

Figure 16. Superelastic stress-strain curves obtained with the multilinear model compared with their experimental counterparts. (a) Set of parameters P1 from table 1. (b) Set of parameters P2 from table 1.

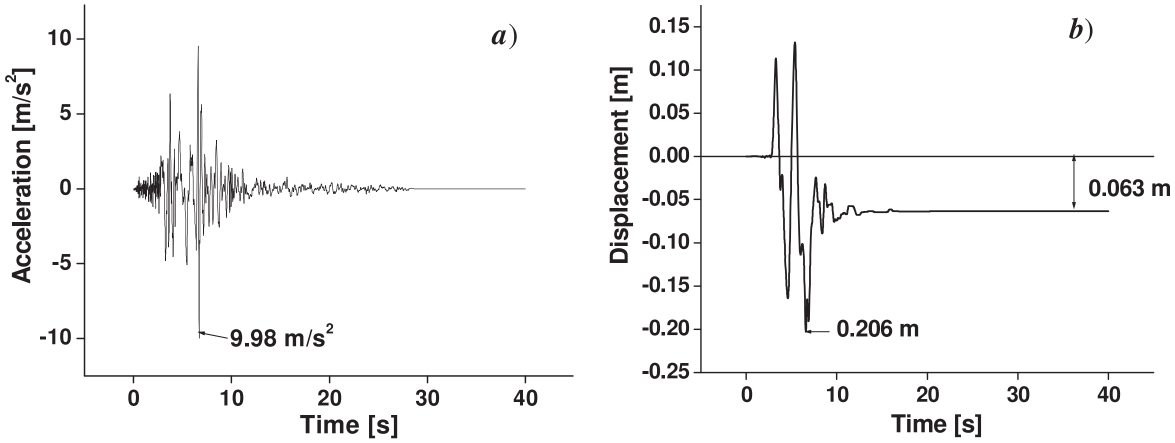

Figure 17. (a) Accelerogram used for the analysis corresponding to the Northridge earthquake, 17 January 1994 [34]. (b) Displacement response of the model structure with the prototype not included.

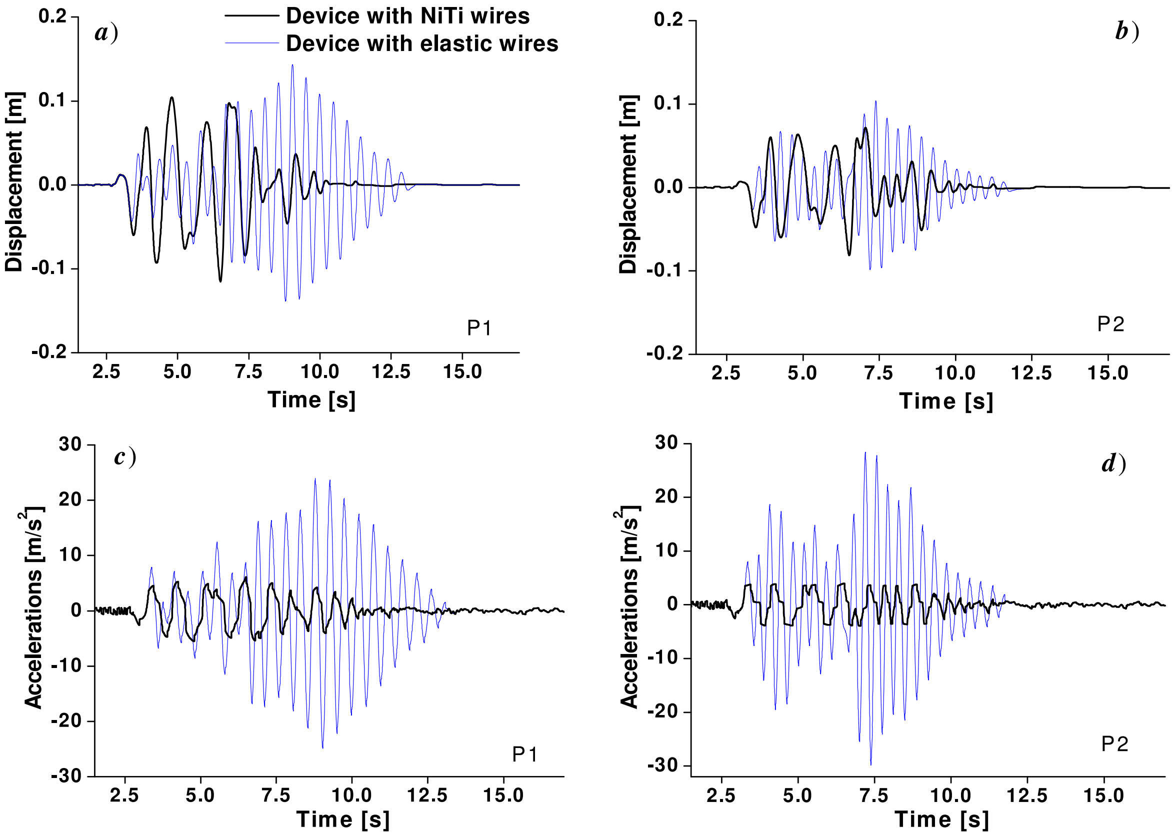

Figure 18. Simulated dynamical response: relative mass displacements for P1 (a) and P2 (b); absolute accelerations for P1 (c) and P2 (d).

obtained with fully elastic devices, for which ground acceleration results amplified reaching values up to 30 m s^{-2}.

The resultant F–X diagrams are shown in figures 19(a) and (b). It is observed that the NiTi wires are effectively strained in their superelastic regime. The forces exerted by the devices can also be distinguished from those due to friction. Figures 20(a) and (b), in turn, allow one to compare the contributions of the device strain work and the friction to the input energy dissipation for P1 and P2 respectively. In both cases, the energy dissipated due superelastic hysteretic work is comparable to that dissipated by friction.

5. Summary and conclusions

In the present work, a comprehensive characterization of a device equipped with NiTi superelastic wires capable of providing self-centering force and damping capability to structures subjected to dynamic loading was performed. The

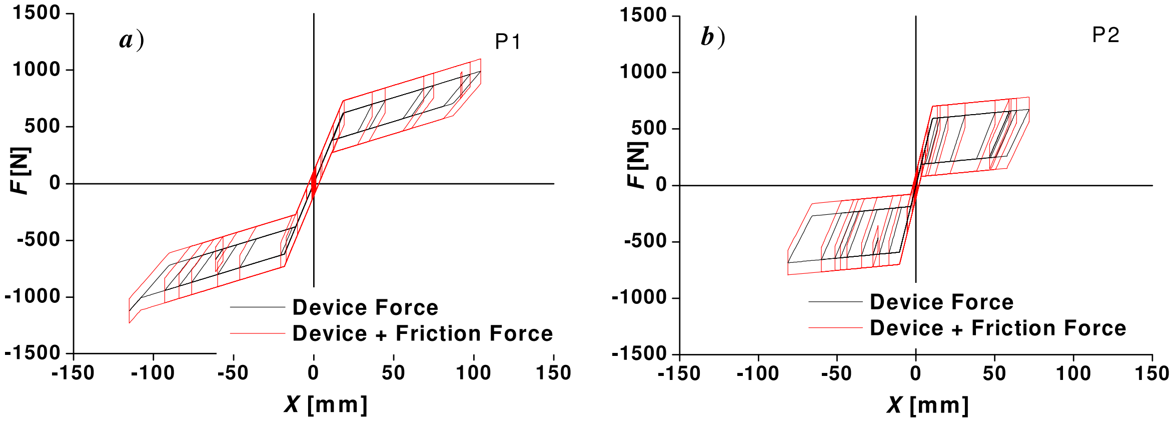

Figure 19. *F*–*X* curves developed during the simulated dynamical responses for (a) the P1 and (b) the P2 set of parameters in table 1.

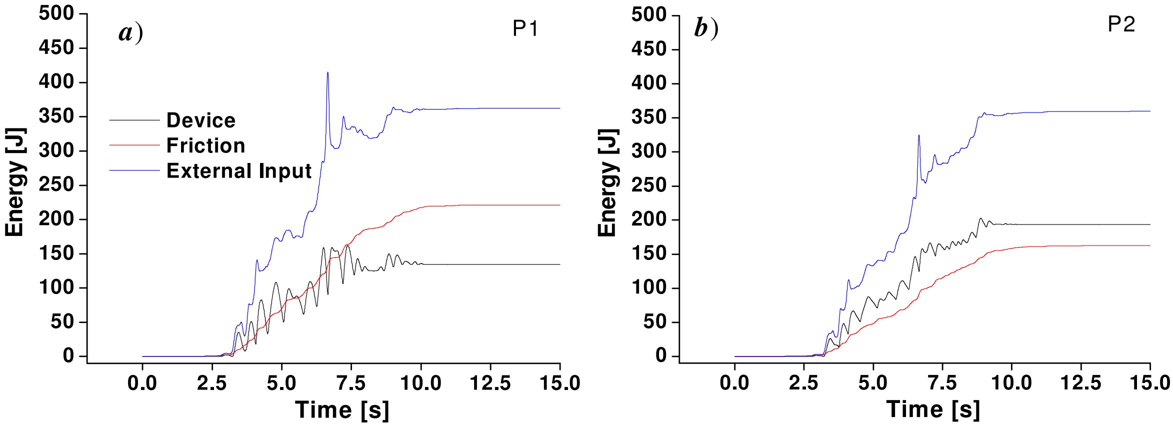

Figure 20. Energy input and dissipative works performed by the superelastic device and the friction of the PTFE layers for (a) P1 and (b) P2.

introduction of pre-straining was shown to be highly beneficial, allowing a correct functioning of the device by avoiding wire loosening or the alternative time costly stabilization training procedures. These benefits could be achieved without sacrificing the self-centering characteristics provided by the superelastic wires.

For all the explored displacement amplitudes, the device exhibited non-monotonic frequency dependence of the hysteresis and of the loss factor. Maximum values of both variables were reached around 0.01 Hz. A linear dependence of the hysteresis energy with the amplitude was found while the loss factor exhibited an approximately constant value for each of the cycling frequencies considered.

A frequency dependence of the superelastic cycles was observed. This could be interpreted in terms of results published elsewhere concerning the thermal effects associated with the first order character of the stress-induced martensitic transformation responsible for the particular behavior of SMAs in general, and NiTi alloys in particular.

Sustained cycling produces changes in the superelastic curves, appreciably at the highest explored amplitudes and frequencies which can also be associated with thermal effects. However, they were not considered for the material model developed here. The characteristics of the responses simulated for the superelastic device (few cycles, diminishing amplitudes) endorse the validity of this assumption, at least for this kind of structural problem.

The numerical time history analysis performed in the present work allowed one to verify the beneficial effect of the superelastic device for a specific structural problem. It acts as a restrainer by limiting maximum and residual displacements of the associated mass. Additionally, the device contributed to the isolation of the mass by reducing the ground accelerations transmitted from the floor to the structure. The analysis of the response obtained with a fully elastic device yielded a similar reduction in the maximum displacements, but the accelerations are highly amplified. This result endorses the beneficial effect of the superelastic device because of its self-centering characteristics as well as its damping characteristics.

Finally, it is worth pointing out that the mass associated with the device *M*, and the wire length *L* were selected arbitrarily, and results may vary with these two design variables. For the sake of brevity, this analysis was limited only to this case for which the device provides a beneficial action as a restrainer and damper. A systematic study is being elaborated, with the aim of defining a multi-objective selection procedure for *M* and *L* according to a determined seismic scenario, which will be a matter of further publications.

Acknowledgments

Funding from project PICT 0898-2011 (ANPCyT), program SECTyP 2010–2014 (UNCuyo) and CNEA is acknowledged. HS also acknowledges CONICET for financial support.

References

[1] Duerig T, Melton M, Stöckel D and Wayman C 1990 *Engineering Aspects of Shape Memory Alloys* 1st edn (London: Butterworth-Heinemann)

[2] Wilson J C, Eeri M and Wesolowskya M J 2005 Shape memory alloys for seismic response modification: a state-of-the-art review *Earthquake Spectra* **21** 569–601

[3] Shaw J and Kyriakides S 1995 Thermomechanical aspects of NiTi *J. Mech. Phys. Solids* **43** 1243–81

[4] Berton S, Infanti S, Castellano M G and Hikosaka H 2007 Self-centring capacity of seismic isolation systems *Struct. Control Health Monit.* **14** 895–914

[5] Cardone D 2012 Re-centring capability of flag-shaped seismic isolation systems *Bull. Earthquake Eng.* **10** 1267–84

[6] Attanasi G, Auricchio and F Fenve G 2009 Feasibility assessment of an innovative isolation bearing system with shape memory alloys *J. Earthquake Eng.* **13** 18–39

[7] Otsuka K and Ren X 2005 Physical metallurgy of Ti–Ni-based shape memory alloys *Prog. Mater. Sci.* **50** 511–678

[8] Iadicola M A and Shaw J A 2007 An experimental method to measure initiation events during unstable stress-induced martensitic transformation in a shape memory alloy wire *Smart Mater. Struct.* **19** 155–69

[9] Attanasi G and Auricchio F 2011 Innovative superelastic isolation device *J. Earthquake Eng.* **15** 72–89

[10] Ozbulut O, Hurlebaus S and Desroches R 2011 Seismic response control using shape memory alloys: a review *J. Intell. Mater. Struct.* **22** 1531–49

[11] Yawny A, Sade M and Eggeler G 2005 Pseudo elastic cycling of ultra fine grained NiTi shape-memory wires *Int. J. Mater. Res. (Zeitschrift für Metallkunde)* **06** 608–18

[12] Olbricht J, Yawny A, Condó A M, Lovey F C and Eggeler G 2008 The influence of temperature on the evolution of functional properties during pseudoelastic cycling of ultra-fine grained NiTi *Sci. Eng.* A **481-482** 142–5

[13] Krooß P, Somsen C, Niendorf T, Schaper M, Karaman I, Chumlyakov Y, Eggeler G and Maier H J 2014 Cyclic degradation mechanisms in aged FeNiCoAlTa shape memory single crystals *Acta Mater.* **79** 126–37

[14] Saadat S, Noori M, Davoodi H, Hou Z, Suzuki Y and Masuda A 2001 Using NiTi SMA tendons for vibration control of coastal structures *Smart Mater. Struct.* **10** 695–704

[15] Barrata A and Corbi O 2002 On the dynamic behaviour of elastic–plastic structures equipped with pseudoelastic SMA reinforcements *Comput. Mater. Sci.* **25** 1–13

[16] Tanaka Y, Himuro Y, Kainuma R, Sutou Y, Omori T and Ishida K 2010 Ferrous polycrystalline shape-memory alloy showing huge superelasticity *Science* **327** 1488–90

[17] Omori T, Abe S, Tanaka Y, Lee D Y, Ishida K and Kainuma R 2013 Thermoelastic martensitic transformation and superelasticity in Fe–Ni–Co–Al–Nb–B polycrystalline alloy *Scr. Mater.* **69** 812–5

[18] de Castro Bubani F, Sade M and Francisco Lovey F C 2012 Improvements in the mechanical properties of the 18R ↔ 6R high-hysteresis martensitic transformation by nanoprecipitates in CuZnAl alloys *Mater. Sci. Eng.* A **543** 88–95

[19] DellVille R, Malard B, Pilch J, Sittner P and Schryvers D 2010 Microstructure changes during non-convectional heat treatment of thin Ni-Ti wires by pulsed electric current studied by transmission electron microscopy *Acta Mater.* **58** 4503–15

[20] Dolce M, Cardone D and Marnetto R 2001 SMA recentering devices for seismic isolation of civil structures *Proc. SPIE* **4330** 238

[21] Dolce M, Cardone D, Ponzo F C and Valente C 2005 Shaking table tests on reinforced concrete frames without and with passive control systems *Earthquake Eng. Struct. Dyn.* **34** 1687–717

[22] Parulekar Y M, Reddy G R, Vaze K K, Guha S, Gupta C, Muthumani K and Sreekala R 2012 Seismic response attenuation of structures using shape memory alloy dampers *Struct. Control Health Monit.* **19** 102–19

[23] Han Y, Xing D, Xiao E and Li A 2005 NiTi-wire shape memory alloy dampers to simultaneously damp tension, compression and Torsion *J. Vib. Control* **11** 1067–84

[24] Speicher M, Hodgson D E, DesRoches R and Leon R 2009 Shape memory alloy tension/compression device for seismic retrofit of buildings *J. Mater. Eng. Perform.* **18** 746–53

[25] Soul H, Isalgue A, Yawny A, Torra V and Lovey F C 2010 Pseudoelastic fatigue of NiTi wires: frequency and size effects on damping capacity *Smart Mater. Struct.* **19** 085006

[26] Soul H and Yawny A 2010 Thermomechanical model for evaluation of the superelastic response of NiTi shape memory alloys under dynamic conditions *Smart Mater. Struct.* **22** 035017

[27] He Y J and Sun Q P 2011 On non-monotonic rate dependence of stress hysteresis of superelastic shape memory alloy bars *Int. J. Solids Struct.* **48** 1688–95

[28] Paradis A, Terriault P, Brailovski V and Torra V 2008 On the partial recovery of residual strain accumulated during an interrupted cyclic loading of NiTi shape memory alloys *Smart Mater. Struct.* **17** 065027

[29] Carfagni M, Lenzi E and Pierini M 1998 The loss factor as a measure of mechanical damping *IMAC XVI: 16th Int. Model Analysis Conf.* pp 580–4

[30] Ashby M F 2011 *Materials Selection in Mechanical Design* (London: Elseiver) pp 165–8

[31] American Association of State Highways and Transportation Officials (AASHTO) 1999 *Guide Specifications for Seismic Isolation Design* (Washington, DC: American Association of State Highways and Transportation Officials)

[32] He Y J and Sun Q P 2010 Frequency-dependent temperature evolution in NiTi shape memory alloy under cyclic loading *Smart Mater. Struct.* **19** 115014

[33] Heller L, Sittner P, Pilch J and Landa M 2009 Factors controlling superelastic damping capacity of SMAs *J. Mater. Eng. Perform.* **18** 603–11

[34] Erot M 2007 Advanced models for sliding seismic isolation and applications for typical multi-span highway bridges *PhD Thesis* Georgia Institute of Technology

[35] Chopra A K 1985 *Dynamics of Structures* (Englewood Cliffs, NJ: Prentice-Hall) p 164

[36] Pacific Earthquake Engineering Research 2000 PEER Strong Motion Database http://peer.berkeley.edu/smcat